UTP-
11-06-96

Four-dimensional pure compact U(1) gauge theory on a spherical lattice

J. Jersák

Institut für Theoretische Physik E,
RWTH Aachen, Germany

C. B. Lang

Institut für Theoretische Physik,
Karl-Franzens-Universität Graz, Austria

T. Neuhaus

FB8 Physik, BUGH Wuppertal, Germany

February 1, 2008

arXiv:hep-lat/9606013v1 22 Jun 1996

Abstract

We investigate the confinement-Coulomb phase transition in the four-dimensional (4D) pure compact U(1) gauge theory on spherical lattices. The action contains the Wilson coupling β and the double charge coupling γ. The lattice is obtained from the 4D surface of the 5D cubic lattice by its radial projection onto a 4D sphere, and made homogeneous by means of appropriate weight factors for individual plaquette contributions to the action. On such lattices the two-state signal, impeding the studies of this theory on toroidal lattices, is absent for $\gamma \leq 0$. Furthermore, here a consistent finite-size scaling behavior of several bulk observables is found, with the correlation length exponent ν in the range $\nu = 0.35 - 40$. These observables include Fisher zeros, specific-heat and cumulant extrema as well as pseudocritical values of β at fixed γ. The most reliable determination of ν by means of the Fisher zeros gives $\nu = 0.365(8)$. The phase transition at $\gamma \leq 0$ is thus very probably of 2^{nd} order and belongs to the universality class of a non-Gaussian fixed point.

1 Introduction

1.1 Motivation

The introduction of a space-time lattice for quantum field theories serves several purposes. It provides a regularization for the renormalization scheme; it allows us to apply efficient computational methods to perform the functional integrals; it may be considered a mere approximation scheme for the problem in the continuum. Among the four-dimensional (4D) gauge field theories with Lie groups the one with $U(1)$ symmetry at first sight appears to be the simplest to test this approach. It is also of considerable interest as it has many features in common with QCD, like a confining strong coupling phase, topological excitations and gauge-balls. In addition it shows a phase transition (PT) to a phase with weak coupling signature, a massless photon and long range interaction. In fact it has been the first lattice gauge model with continuous gauge group to be studied by the computational methods that became available in the 80's [1].

Below (in subsect. 1.2) we will discuss the various results obtained since. However, in summary we may say that up to now there is no definite answer to the critical properties of its PT. In most simulations a two-state signal at the PT indicated a $1^{\rm st}$ order transition. On the other hand, the critical behavior according to such a transition has not been confirmed in thorough finite-size scaling (FSS) studies. The problem persisted when the original Wilson action containing only $\cos(\Theta_P)$ was extended to include the double charge coupling

$$S = -\sum_P \left(\beta\cos(\Theta_P) + \gamma\cos(2\Theta_P)\right). \tag{1}$$

Here $\Theta_P \in [0, 2\pi)$ is the plaquette angle, i.e. the argument of the product of $U(1)$ link variables around a plaquette P. It was conjectured, that the $1^{\rm st}$ order PT changes into a $2^{\rm nd}$ order one at a tricritical point (TCP) at small negative values of γ, but that was never confirmed in actual simulations at $\gamma \leq 0$. If there is indeed a $2^{\rm nd}$ order transition, its properties have not been determined up today.

On the other hand, both computational and data analysis techniques have progressed. This provides us with the possibility to perform a thorough FSS study of this model in a new context. Practically all other studies have dealt with the standard periodic boundary conditions, i.e. hypertorus topology for

the lattices. It has however been realized that there are nonlocal excitations in the system — closed monopole loops — that may extend over the whole lattice. Therefore the essentially local updating algorithms used for gauge theories, together with the boundary conditions, may affect thermalization properties. One expects, that in the thermodynamic limit the "continuum" properties of the system are independent of the global topology of the system, if this becomes locally flat. For these reasons it was suggested to simulate the model on lattices with spherelike topology [2], amounting to modified boundary conditions, such that closed loops are always homotopically equivalent to points. The spherelike topology allows the monopoles more freedom in their dynamics without changing the action.

One generally expects that the thermodynamic properties of the bulk phase (defined by the behavior of the free energy per unit volume in the thermodynamic limit) are not affected by contributions which grow slower than the total volume. Boundary contributions are suppressed $O(1/L)$ relative to the leading term, curvature terms at least $O(1/L^2)$, and therefore they should not change the critical exponents of the bulk phase. This does not necessarily hold for the ground state. E.g. at phase transitions of 1^{st} order the phase mixture may be different, depending on boundaries or even one individual spin, or due to an overall external field vanishing $O(1/L^D)$. A similar influence may come from the curvature, even if thinned out over the volume in $O(1/L^2)$. However, if the manifold becomes locally flat in the thermodynamic limit the systems universal *critical* properties should be independent of the global topological structure. Otherwise we could hardly assume that we can do reliable physics on earth without definite knowledge about the topological details of the universe.

Whereas in the original study [2] the surface of a 5D cube was used, we here choose a discretization of the sphere, where the curvature is distributed more homogeneously over the lattice. Although the system is nonhomogeneous on the scale of the lattice constant, it is homogeneous and isotropic on larger scales. As will be demonstrated here, in this 4D system with the topology of the surface of a 5D sphere we find no two-state signal on lattices with up to almost 20^4 points. Of course we cannot exclude the possibility, that a two-state signal reappears for even larger lattices. However, our FSS analysis leads to consistent results for a PT of 2^{nd} order for $\gamma \leq 0$.

The best measurement of the correlation length critical exponent ν by means of the FSS behavior of the Fisher zero gives $\nu = 0.365(8)$. Less precise FSS analyses of several other bulk observables are consistent with ν

values in the interval $\nu = 0.35 - 0.40$. As we argue in [3], due to rigorous dual relationships our results imply that also the Coulomb gas of monopole loops[4] and the noncompact U(1) Higgs model at large negative squared bare mass (frozen superconductor)[5] have a continuum limit described by the same non-Gaussian fixed point. Some further related models are discussed in [6].

The first order signal persists — also for the discussed spherelike geometries — at values $\gamma \simeq 0.2$. Since scaling may be garbled close to TCPs we concentrated on negative values of the double charge coupling γ in our study. Scaling and FSS is expected to improve at larger distance from the $1^{\rm st}$ order part of the PT line. Nevertheless, at $\gamma = 0$ the two-state signal is still absent and the scaling behavior is consistent with that found at $\gamma < 0$.

Let us add a remark on the extended action considered. Some time ago it was pointed out [7], that, although the Wilson- and the heat kernel (Villain) action do have reflection positivity, some actions do not. Positivity is a sufficient, but not a necessary condition for unitarity; it guarantees the existence of a positive definite scalar product and the spectral condition, one of the formal conditions for the existence of a continuum limit field theory [8]. The actions with the parameter values $\gamma < 0$ considered here are not reflection positive. They share this property with other actions like e.g. the (Symanzik) improved actions.

On the other hand, if reflection positivity holds on a part of a critical surface that is in the domain of attraction of a fixed point of some renormalization group transformation, we expect that it should be fulfilled everywhere in that domain. Unitarity violating states like ghosts should then decouple at large scale. We therefore find it justified to study the action near candidates for critical points even outside the region $\gamma \geq 0$, where reflection positivity is respected on the scale of the lattice spacing. Unitarity at $\gamma < 0$ is also suggested by the observation that the regions with $\gamma < 0$ and $\gamma \geq 0$ are connected by the RG flows [9].

Following a brief review of the situation in the U(1) pure gauge model we then introduce the spherical lattice in sect. 2. (Further technical details are given in the appendix.) In sect. 3 we present the Monte Carlo simulation and discuss the observables in some detail, including the expected FSS behavior. The results and their analysis are summarized in sect. 4, followed by our conclusions.

1.2 Situation of U(1) pure gauge studies

U(1) is the most elementary Lie group that can be used to construct a quantum gauge field theory. Yet, when formulated on a lattice, the pure U(1) gauge theory turned out unexpectedly to be one of the most intriguing and less understood quantum gauge models. The awareness of this fact has developed with an accumulation of the numerical experience. In this section we give a brief description of this historical development. We apologize for quoting only a subjectively chosen part of a much larger number of valuable papers.

Since the introduction of lattice gauge theories by Wilson [10], the pure compact U(1) theory has been of interest as a theory with a rigorously established [11, 12] PT between the confinement and the free charge (Coulomb) phases at zero temperature. One reason was the importance of topological excitations, the monopoles, for confinement, as manifested by their prominent rôle in this phase transition [4, 13, 14, 15, 16, 17]. Another purpose was to study it as a prototype example for applications of numerical methods of statistical physics in a lattice gauge theory, in particular an investigation of the continuum limit at the phase transition. However, the lesson has been that this phase transition provides no simple exercise.

In the very first numerical investigations [1, 18, 19, 20, 21], restricted to $\gamma = 0$ and small lattices, a behavior consistent with a $2^{\rm nd}$ order phase transition at $\beta \simeq 1$ was observed. But this order was questioned by the subsequent observation of a two-state signal on larger lattices [22]. Such a signal could imply that the phase transition at $\gamma = 0$ is actually of weak $1^{\rm st}$ order, which would prevent taking a continuum limit there. The question was, and remained to be, whether this signal may be a finite-size effect.

In the model with extended Wilson action (1) it was found [23] that the confinement-Coulomb phase transition is clearly of $1^{\rm st}$ order for $\gamma \geq 0.2$, and weakens with decreasing γ. This suggested that the order of the transition changes when γ is decreased, presumably at a TCP.

The question at which value of γ this happens turned out to be very difficult. First, even at large negative γ, a two-state signal has been observed, e.g. at $\gamma = -0.5$ on the 8^4 lattice [24]. Second, TCPs are known to cause intricate finite-size effects [25], easily mocking up a false order of the phase transition.

In the hope to clarify the situation, an investigation of the strongly $1^{\rm st}$ order part of the phase transition line at $\gamma \geq 0.2$ was performed [24]. There

the latent heat Δe can be determined reliably even on moderately large lattices. Its independence on the lattice size was checked very carefully. The extrapolation of Δe to zero with decreasing γ by means of the power law

$$\Delta e \propto (\gamma - \gamma^{TCP})^{\beta_u}, \tag{2}$$

suggested that the order of the transition changes at the TCP with $\gamma^{TCP} = -0.11(5)$, implying a $1^{\rm st}$ order PT at $\gamma = 0$.

This extrapolation procedure is an attempt to control finite-size effects, but it uses the assumption that the power law behavior (2), which the data in the investigated region $\gamma = 0.2 - 0.5$ are consistent with, indeed holds throughout the whole interval between $\gamma = 0.5$ and $\gamma = \gamma^{TCP}$. This assumption has remained unverified. Another possible uncertainty in [24] was the determination of Δe at a strong $1^{\rm st}$ order transition, without the more advanced methods of investigation of such transitions [26].

Monte Carlo RG (MCRG) studies [27, 28, 9, 29] did not confirm this position of the TCP at negative γ. Of course, also the MCRG approach suffers from ambiguities due to a small number of RG steps and a restricted number of couplings considered. Therefore also these studies remained inconclusive about the order of the transition around $\gamma = 0$ in the thermodynamic limit (although they all observed clear two-state signals).

In spite of this, numerous attempts to determine the critical exponent ν provided roughly consistent values in the range $\nu \simeq 0.28 - 0.42$. These studies used various methods: the analytic calculations [30, 31], the FSS analysis [18, 19, 23, 32], the scaling of the string tension [20, 33, 34, 35], and the MCRG method [27, 28, 9, 36, 29]. Three actions: Wilson–, extended Wilson–, and Villain–type have been used.

This suggested that the pure compact U(1) lattice theory might have an interesting continuum limit at the confinement-Coulomb PT, pondered, e.g., in [5, 37]. However, the two-state signal, observed on finite lattices even for $\gamma < 0$ [24] as well as for the Villain action [36], hindered the investigations of this possibility. Even if this signal is only a finite-size effect and the transition in the infinite volume limit is genuinely of $2^{\rm nd}$ order, it represents a serious impediment for a precise FSS analysis or MCRG studies. Because of this the investigation of the pure compact U(1) gauge theory lost its momentum. Until now there is no established $2^{\rm nd}$ order PT with an undisputed determination of critical indices in this model.

All the above mentioned numerical work has been performed on 4D toroidal lattices. Recently, following earlier suggestions [38, 28, 9], two of

the present authors speculated that the two-state signal at $\gamma \leq 0$ may be related to monopole loops winding around the toroidal lattice, and trapped in simulations with local update algorithms [2]. They used the 4D surface of a 5D cubic lattice instead of the torus, and observed that at $\gamma = 0$ the two-state signal vanishes on lattices of all investigated sizes.

Choosing a spherelike topology provides a way to allow the monopoles more freedom in their dynamics without affecting them locally by changing the action. We consider this as preferable to adding terms to the action that forbid or restrict the occurrence of monopoles produces $O(L^D)$ contributions to the total free energy and thus changes the bulk properties of the system [39, 40]. In that case one explores the phase diagram in different regions of the space of couplings and the position of the phase transition in β moves to different values, depending on the extra couplings. None of these studies has led to phase transitions of 2^{nd} order, though.

However, the cause for the two-state signal on the toroidal lattice, and of its vanishing on a lattice with the topology of a sphere, is not yet fully understood. Possibly the trivial 1^{st} homotopy group of such a lattice allows a smooth vanishing of winding monopole loops in simulations. But some other recent results do not seem to support this interpretation [40, 41, 42].

On the other hand, for a study of the continuum limit on lattices with the topology of a sphere, a complete understanding of the dynamics of the two-state signal on a torus is not really necessary. What is required is a construction of a spherelike lattice which is homogeneous, in order to avoid the possibly related problems with the FSS analysis, encountered in [2]. Achieving that in this paper, we hope to give a new momentum to the investigation of the confinement-Coulomb phase transition in the pure compact U(1) gauge theory on the lattice. A construction of the continuum limit appears now to be feasible.

2 Spherelike lattices and lattice geometry

In an attempt to formulate the theory without modification of the locally defined plaquette action and without forbidding or hindering the dynamic evolution of monopole loops, the lattice topology was modified. The usual periodic (or antiperiodic) boundary conditions correspond to the topology of a 4D torus T^4 with the first homotopy group $\mathbf{Z}^4$. Closed loops (or networks of loops) cannot necessarily be contracted to a point and the corresponding

ground state may be classified accordingly. The original motivation to divert from this lattice structure was to study the possible influence of this property on the dynamics of the phase transition.

In [2] it was therefore suggested to simulate and study the model on a lattice with spherelike topology, in particular on the surface SH[N] of a 5D hypercubic lattice of size N^5. This lattice may be best visualized in analogy to the 2D surface of a 3D cubic lattice. It may also be considered as a collection of 10 hypercubic lattices of size N^4, glued together at their boundaries. This implies that one can expect the same critical coupling in the thermodynamic limit as for the usual torus. This was indeed verified in the Monte Carlo calculations [2]. Details and parameters of the geometry are listed in the appendix.

The so-defined lattice is locally flat, except at certain plaquettes ((D-2)-dimensional elements), where the curvature is concentrated, a well-known property of Regge skeletons. The unusual features include plaquettes bordering only three 3D cubes (instead of the usual 4), links bordering less than 6 plaquettes and sites with less than 8 links. These curvaturelike contributions as we might call them in the absence of a strict theory in 4D are suppressed $O(1/N^2)$ relative to the leading terms in the action.

In an attempt to distribute these local inhomogeneities more uniformly over the lattice we introduced the "almost smooth" spherical lattice S[N]. In the construction we project sites, links and plaquettes of SH[N] (or its dual SH'[N]) onto the surface of a concentric 4D sphere and introduce weight factors similar to those used by [43] in their study of random triangulated lattices,

$$\begin{aligned} S &= -\sum_P w_P[\beta\cos(\Theta_P) + \gamma\cos(2\Theta_P)] \\ &\text{with} \quad w_p = \frac{A'_P}{A_P}. \end{aligned} \tag{3}$$

Here, A_P and A'_P denote the areas of the corresponding plaquette and its dual, respectively, of the projected lattice.

As discussed in [43] in the situation of triangulated random lattices, one has to distribute the total integration volume over all contributions to the action, i.e. the plaquette terms in our case. This may be done with the help of the dual lattice, where to each site, link or plaquette there is an associated dual 4D cube, 3D cube or plaquette. The dual lattice sites in our situation are constructed from the barycenters of the 4D cubes that have been projected

to the sphere S^4, followed by an adjusting projection of these points to the sphere. Further reasoning according to [43] leads to the weight factors w_P in (3). This choice is not unique, but reproduces the usual continuum action $F_{\mu\nu}^2$ in the naive continuum limit $g \to 0$ ($\beta \to \infty$) and is thus homogeneous in this limit. We study the system at finite β; there slight distortions from the regular spherical surface are possible. The value of β_{crit} might be modified due to the weight factors and thus does not necessarily agree with that of the torus or SH.

Technically we have to introduce some approximations. Usually the plaquettes – constructed via the projection of the sites to the sphere – will not be flat. Plaquette areas are therefore determined from the sum of two triangles. Also for this reason the curvature in this formulation will not be perfectly uniformly distributed. In order to achieve this, we would have to rely on a triangulated lattice. This would imply a significant change of the action, which we wanted to avoid. On the other hand we expect these effects to become irrelevant in a situation with a large correlation length. The consistency of the found FSS behavior justifies these simplifications.

The connectivity properties of SH and S are identical. In the computer programs the geometry is implemented with tables and the weight factors w_P are precalculated. During the development of the program and in the early stages of the analysis we also determined the monopole positions (on the dual lattice) and reproduced them graphically. We observed the expected properties:

- The monopole loops were always closed;
- the smallest loops had length 3 (corner plaquettes on the dual lattice);
- they fluctuated freely, appearing and disappearing without noticeable correlation with positions close to corners.

This also served as a check of the consistency of the connectivity tables.

In our discussions we will refer to the *effective* lattice volume

$$V = \frac{1}{6} \sum_P w_P \tag{4}$$

as the typical size quantity. For SH this would be just the number of sites, for S it is very close to this value. A length scale may be defined as

$$L \equiv V^{\frac{1}{4}}. \tag{5}$$

Table 1: Effective volumes for the studied lattices SH[N]. We also give the value of $L = V^{\frac{1}{4}}$ which would give the base length for a hypertorus lattice with the same volume.

N	V	L
4	825.1	5.4
5	2576.6	7.1
6	6268.1	8.9
7	12986.9	10.7
8	24064.1	12.5
9	41074.6	14.2
10	65837.3	16.0
12	147113.8	19.6

Table 1 summarizes the effective volumes for the lattice sizes used in our study.

For strictly asymptotic dependencies as they come up in FSS studies it is irrelevant, whether one uses N or L. However, for moderately sized finite systems a suitable choice improves the approach to the asymptotic behavior. Let us mention in this context that in [44] different lattice geometries were compared and it was demonstrated, that the scaling curves show best agreement with each other, if one indeed uses L – the size derived from the total volume as opposed to the base length N – as size variable. In the present work we cannot compare with torus results, since for those the two-state signal obscures the measured values of the cumulants.

3 Simulation methods and statistics

In an earlier study [2] we found that for lattice type SH there are two-state signals at the pseudocritical β for $\gamma = 0.2$, but no such indications at $\gamma = 0$. For this reason we now studied the action (3) of the spherical lattice S at the values $\gamma = 0., -0.2, -0.5$. Preliminary results have been presented in [45, 46].

3.1 Updating and measuring

We have worked with lattices S[N] for N ranging between 4 and 12. The couplings were chosen in the immediate neighborhood of the pseudocritical values of β. For the analysis we determined the histograms of the weighted sum of plaquette values

$$E \equiv \sum_P w_P \cos \Theta_P. \tag{6}$$

Note that this is not the total energy, but just the part corresponding to the coupling parameter β; it coincides with the total plaquette energy for the Wilson action, $\gamma = 0$. Any scaling- or two-state signal should be observable in that quantity. We also define the density

$$e \equiv E/\sum_P w_P = E/(6V). \tag{7}$$

We combined the various histograms (for fixed γ but different β) with help of the Ferrenberg-Swendsen multihistogram reweighting technique [47]. For each γ we thereby construct the density of states $\rho(E;\gamma)$. The representation

$$Z(\beta,\gamma) \equiv \sum_E \rho(E;\gamma) \exp\left(-\beta E\right) \tag{8}$$

allows us to determine various observables for continuous values of β through

$$\langle E^n \rangle = \frac{1}{Z(\beta,\gamma)} \sum_E \rho(E;\gamma) E^n \exp\left(-\beta E\right). \tag{9}$$

Since we never observed two-state signals we did not implement multicanonical updating [26]. We used a 3-hit Metropolis update; for $\gamma = 0$ we included an additional overrelaxation step (the autocorrelation length decreased by a factor of about 2). For each lattice size at each γ we typically accumulated $O(10^6)$ updates, which is between 10^3 and 10^4 times the integrated autocorrelation length for the observable E (cf. Table 2).

The histograms had up to 10^4 bins in order to exclude any possible influence due to binning. In fact, by rebinning we found no changes within single precision down to $O(500)$ bins. Due to the fine binning the raw histograms have a noisy appearance, which is irrelevant for the Ferrenberg-Swendsen analysis and for the representation (8). For the plots we use rebinned versions with only 500 bins maximum.

The total CPU-time spent for the calculations on workstations and on a Cray-YMP sums up to 6800 hours in Cray-YMP units.

Table 2: Statistics of the data for the studied values of γ: Lattice base length N, total number n of configurations in multiples of 10^6, range of β-values, maximal τ_{int} values (from a fit to all beta values, as discussed in the text; errors are typically 10% of the values).

γ	N	$n/10^6$	β-range	$\tau_{int,max}$
0.	4	1.1	0.98—1.025	12
	6	1.0	1.—1.025	56
	8	1.1	1.0125—1.0275	150
	10	1.47	1.01—1.025	304
-0.2	4	1.1	1.07—1.2	24
	5	1.8	1.15—1.175	63
	6	1.6	1.13—1.21	116
	7	1.1	1.14—1.175	188
	8	1.6	1.155—1.175	272
	9	1.1	1.1655—1.1715	367
	10	1.0	1.1635—1.1715	583
-0.5	4	4.8	1.3—1.65	37
	5	1.8	1.38—1.47	76
	6	2.1	1.35—1.5	149
	7	1.9	1.402—1.452	311
	8	1.5	1.4—1.455	332
	9	1.8	1.42—1.442	480
	10	1.55	1.42—1.442	473
	12	1.6	1.43—1.44	1565

3.2 Observables and FSS

3.2.1 Cumulants

We determined the 2^{nd} and 4^{th} order cumulants of the observable E. Due to the analogy to the internal energy (identical to E only for $\gamma = 0$) we call the second order cumulant the specific-heat. The specific-heat, the Challa-Landau-Binder cumulant [48] and another 4^{th} order cumulant suggested by Binder (cf. [49] and [50]) are defined through

$$c_V(\beta, L) \quad = \quad \frac{1}{6V}\langle (E - \langle E \rangle)^2 \rangle, \tag{10}$$

$$V_{CLB}(\beta, L) = -\frac{1}{3}\frac{\langle (E^2 - \langle E^2 \rangle)^2 \rangle}{\langle E^2 \rangle^2}, \tag{11}$$

$$U_4(\beta, L) = \frac{\langle (E - \langle E \rangle)^4 \rangle}{\langle (E - \langle E \rangle)^2 \rangle^2}. \tag{12}$$

The positions and values of their respective extrema are used for the FSS analysis.

From the usual scaling hypothesis [51, 52, 53, 54, 55] one expects for the singular part of the free energy density the scaling behavior

$$f(\tau, L) = L^{-1/D} f(\tau L^{1/\nu}, 1), \tag{13}$$

where $\tau \equiv (1 - \beta/\beta_c)$ denotes the reduced coupling and L is a length scale parameter. From this one derives the scaling behavior of the cumulants. At a 2^{nd} order phase transition we expect (for D=4 and $\alpha > 0$)

$$c_{V,max}(L) \simeq L^{\alpha/\nu}, \tag{14}$$

$$V_{CLB,min}(L) \simeq L^{\alpha/\nu - 4}, \tag{15}$$

$$U_{4,min}(L) \simeq O(1) + O(L^{-\alpha/\nu}), \tag{16}$$

$$\beta_c(L) - \beta_c \simeq L^{-\lambda}. \tag{17}$$

For $\alpha = 0$ there are logarithmic terms. The asymptotic value of $U_{4,min}$ depends on the details of the distribution density $\rho(E)$ and is 3 for a Gaussian distribution. Mean field values are $\nu = 1/2$ and with Josephson's law $\alpha = 2 - D\nu = 0$.

We denote by $\beta_c(L)$ definitions for pseudocritical points like the positions of the extrema in the cumulants. The so-called shift-exponent λ is for many models equal to $1/\nu$, but not necessarily so in general; such an identity is not a necessary result of FSS (cf. the discussion in [55]). We return to this issue later. Furthermore, a priori we know nothing about the absolute size of the multiplicative coefficients in the scaling formulas. They depend on the details of the action, the lattice geometry and the topology [55].

For 1^{st} order transitions one expects the FSS behavior

$$L^{-D} c_{V,max} \to \frac{1}{4}(e_o - e_d)^2, \tag{18}$$

$$V_{CLB,min} \to -\frac{1}{12}\frac{(e_o^2 - e_d^2)^2}{(e_o e_d)^2} + O(L^{-D}), \tag{19}$$

$$U_{4,min} \to 1 + O(L^{-D}), \tag{20}$$

$$\beta_c(L) - \beta_c = O(L^{-D}). \tag{21}$$

Here e_o and e_d denote the discontinuous values of the energy density at the PT point.

As discussed, in the considered lattice geometry there are inhomogeneities in the sense, that the coordination numbers of some sites, links and plaquettes deviate from the usual torus numbers. For the SH lattices these may be considered as lattice inhomogeneities. Their contribution to the total free energy is suppressed $O(1/N^2) = O(V^{-2/D})$. In our smoothed version of that lattice: S, the inhomogeneous contribution should be smaller. There is however still a possible contribution of the total curvature to the free energy, which is suppressed with the same order (cf. also the discussion for the 2D Ising model [44]). Thus — in principle – we also may expect "surface" corrections of $O(V^{-2/D})$ in all FSS relations. Indeed such contributions have been observed for the SH lattices [2]. It turns out that they are much smaller in our present study, in fact too small to study them.

3.2.2 Fisher zeros

Equation (8) defines implicitly an analytic continuation to complex values of β not too far away from the real axis. Therefore it is possible to determine the nearby zeros of the partition function [56] in the complex β-plane, the so-called Fisher zeros [57] (cf. [58]).

One should add a warning concerning technical aspects. The histograms are binned, having both, upper and lower limits for E_{max} and E_{min} as well as a bin size $\Delta = (E_{max} - E_{min}) \times 10^{-4}$. The representation (8) for $\beta = \beta_R + i\beta_I$ therefore is a discrete Fouriertransformation. It will induce a periodicity in β_I due to the bin size and an effective grid with grid spacing $2\pi/(E_{max} - E_{min})$ (although the values of the partition function Z are well-defined even between the grid points, they carry no additional information).

Usually the distribution is similar to a Gaussian distribution; let us for the sake of the argument assume such a form

$$\rho(E) \exp\left(-\beta_R E\right) \simeq \exp\Big(-c(E - E_0)^2\Big). \tag{22}$$

From (8) one then expects an oscillatory behavior of Z proportional to $\exp\left(i\beta_I E_0\right)$. This is indeed observed in the calculation. In the search for partition function zeros one starts with an identification of sign changes of $\mathrm{Im}\, Z$ and $\mathrm{Re}\, Z$. The rapidly oscillating phase factor may confuse the pattern and one has to work with a very fine resolution and to carefully combine

the sign-change analysis with a search in $|Z|$. Also the grid structure may interfere with these oscillations and one has to proceed with care.

So real and imaginary parts of the closest Fisher zeros provide further (even) observables. In particular the imaginary part of the zero closest to the real axis provides a high quality estimator for the critical exponent ν (cf. [59] for a recent high statistics study of the 4D Ising model, where it was possible to identify the logarithmic corrections to scaling on basis of the Lee-Yang zeros [56]). As will be demonstrated below this quantity appears to have small corrections to the leading FSS behavior in our environment; this observation is analogous to other recent investigations of spherelike lattices in 2D [60, 44].

From the scaling arguments for the free energy we expect

$$|z_0(L) - \beta_c| \simeq L^{-1/\nu}. \tag{23}$$

This provides an upper bound for the real and imaginary part of z_0, in particular

$$\begin{aligned} \operatorname{Im} z_0(L) &\simeq O(L^{-1/\nu}), & (24)\\ \operatorname{Re} z_0(L) - \beta_c &\simeq O(L^{-1/\nu}). & (25) \end{aligned}$$

Although in some cases the angle, under which the zeros approach the real axis (defined as the angle of a line connecting the two closest zeros) is known (e.g. $\pi/2$ for the 2D Ising model in the Onsager solution [57], $\pi/4$ in the mean field solution for the 4D ϕ^4-model [61], both on cubic lattices with torus topology) there is no FSS theory for this angle of approach with regard to the size L. Depending on details of the model, the geometry and the topology, the *real part* — which by analogy to the cumulants we call a pseudocritical value — may approach the asymptotic value faster, i.e. with a shift exponent λ larger than $1/\nu$ [55]. Such a behavior has been observed in a recent study of the 2D Ising model [44].

We also mention here, that the position of the closest Fisher zero is related to the peak position and value of the specific-heat. Since the partition function may be expressed by the Vieta-product of all its zeros $\{z_i\}$, the specific-heat is proportional to

$$\sum_i \frac{1}{(\beta - z_i)^2} \tag{26}$$

and therefore the leading contribution to $V \times c_V$ near the PT is proportional to $(\mathrm{Im}\, z_0)^{-2}$. The peak position is in leading order given by $\mathrm{Re}\, z_0$. Of course there are further contributions due to the other zeros and a possible background from an entire function.

Also these observables may in principle exhibit corrections to FSS due to curvature and topology as discussed above.

4 Results and data analysis

4.1 Autocorrelation and error analysis

For all individual runs we determined the integrated autocorrelation for the observable E,

$$\tau_{int,E} = \frac{1}{2} + \sum_{n>0} \frac{\langle E_0 E_n \rangle - \langle E \rangle^2}{\langle E^2 \rangle - \langle E \rangle^2}. \tag{27}$$

(Here the index indicates the n-th configuration measured in the Markov process.) The inverse value provided us with a weight factor of the corresponding data sample in the multihistogram analysis.

For the maximum values of the autocorrelation lengths we produced two sets of values. One was the maximal observed values of $\tau_{int,E}$ for all samples for the given lattice size. The other resulted from a fit to the values of $\tau_{int}(\beta)$ to a peak shaped curve which has its peak position where the specific-heat (see the discussion below of the analysis for the cumulants) assumes its maximum. In the subsequent analysis we discuss only the results due to the first set. The second set led to similar results.

The maximum values of $\tau_{int,E}$ (cf. Table 2) increase from values of $\simeq 12$ for $\gamma = 0, L = 4$ up to $\simeq 1600$ for $\gamma = -0.5, L = 12$. This demonstrates the necessity to work with large samples of several 10^5 configurations for each value of β, at least for the large lattices.

At second order PTs the maximum values of the integrated autocorrelation time provides an estimate for the corresponding dynamical critical exponent z_E through

$$\tau_{int,E} \simeq \min(L, \xi)^{z_E} \tag{28}$$

(where ξ denotes the correlation length). At 1^{st} order transitions one expects that the autocorrelation length grows exponentially $\simeq \exp(cL^{D-1})$. In Fig.1 a log-log plot shows that the size dependence is indeed compatible with (28).

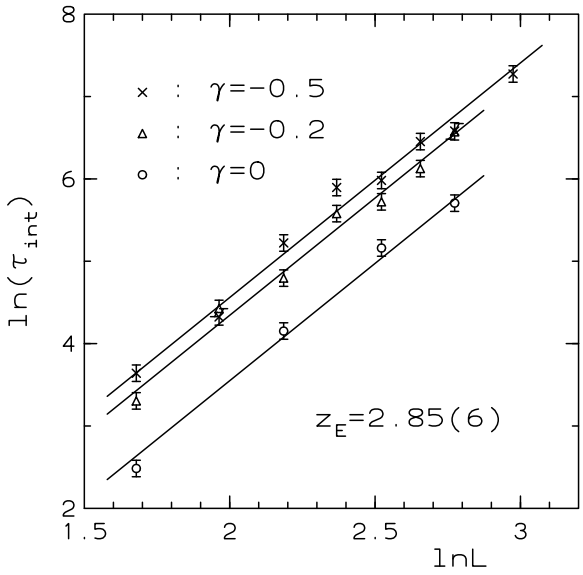

Figure 1: The maximum values of the integrated autocorrelation length for the energy observable together with the fit to an exponential dependence on the lattice size.

We assume, that the peak values correspond to the point where

$$\tau_{int,E}(\beta_{peak}) = c(\gamma) L^{z_E}. \tag{29}$$

A simultaneous fit to all three data sets (for the three values of γ) gives for the dynamical critical exponent $z_E = 2.85(6)$. The coefficients grow from $c(0) = 0.12$ up to $c(-0.5) = 0.32$. The results for $\gamma = 0$ were obtained with an additional overrelaxation step in the Metropolis updating. Although the absolute value of the autocorrelation lengths decreased by a factor of about 2, the dynamical critical exponent appears not to be affected.

That value is substantially larger than the value $z = 2$ expected for the random walk dynamics of local algorithms and demonstrated for Gaussian models. This behavior is indicative of a more complex dynamics than it is usually anticipated for systems with local excitations. The non-locality of the monopole loops may be responsible for the observed effect. On the other hand, we may not yet be asymptotic and the determination of reliable values

for this exponent is notoriously difficult.

As a consistency check we also determined autocorrelation times from a fit to an exponential decay and from blocking analysis. The resulting values were typically proportional to those discussed above, although less reliable, i.e. with large statistical fluctuations. The exponential autocorrelation time and its dynamical critical exponent are upper bounds to the integrated autocorrelation time (cf. [62]).

The statistical errors for all our raw data (i.e. positions and values of cumulant extrema and positions of the Fisher zeros) were determined with the jackknife method. From the original set of values E for each configuration we chose 10 different subsets by omitting 10% of the numbers, providing 10 histograms. The Ferrenberg-Swendsen analysis then was repeated for all these subhistograms and parameters for the cumulants (peak positions, values, Fisher zeros) were determined. The distribution of these numbers defined the errors according to the jackknife procedure. The central values were taken from the analysis of the complete data. The fits were performed using these central values and errors.

The simulations on the CRAY-YMP have been performed employing a vectorized version of the shift-register random number generator, which in its actual implementation uses XOR operations in between the i and $i+103$ element to generate the $i+205$ element of the sequence. For the programs on the workstations we used a corrected version of RCARRY [63] based on the "subtract-and-borrow" version of a lagged Fibonacci algorithm.

4.2 Results: data and fits

We analyzed the final numbers for the pseudocritical points (the extrema positions of the cumulants and the real part of the position of the closest Fisher zero), the extrema values of the cumulants and the imaginary part of the Fisher zero. The fits were performed both, for all lattices sizes and for a subset of lattices with $N \geq 6$, in order to estimate to which amount we see asymptotic behavior.

4.2.1 Histograms

From the combination of histograms determined for different values of β according to the Ferrenberg-Swendsen technique we obtain the distribution densities $\rho(E;\gamma)$ in (8). A necessary condition for the effectiveness of the

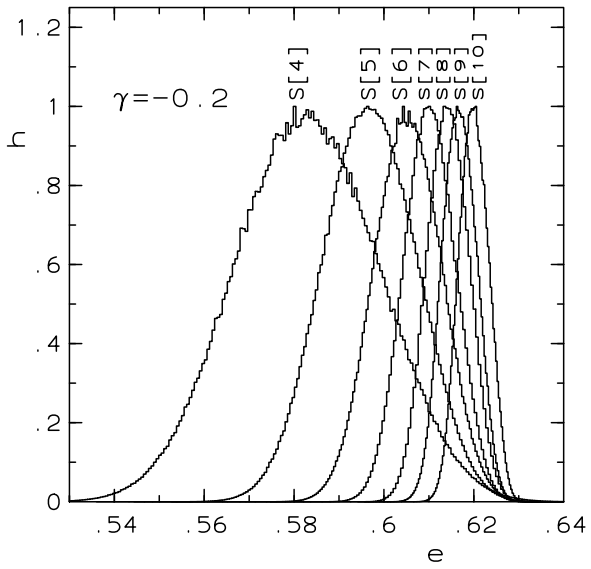

Figure 2: Pseudo-histograms as function of e at $\gamma = -0.2$ and for lattices size N =4, 5, 6, 7, 8, 9, 10 (from left to right) at the respective peak positions of the specific-heat (in Table 3) and normalized to unit maximum value.

approach is sufficient overlap between the individual histograms. From the densities one may construct pseudo-histograms (or reweighted histograms) at arbitrary values of β (which should be in the domain covered by the individual histograms),

$$h(E;\gamma) = \rho(E;\gamma)\exp(-\beta E). \tag{30}$$

These interpolate the individual histograms but they also bring together and represent all histogram data.

In Fig. 2 we plot the pseudo-histograms for $\gamma = -0.2$ for all lattice sizes studied and determined at the peak positions of the specific-heat. They are normalized to unity at their respective maxima. No double peak structure is observable. In Fig. 3 the pseudo-histograms for the largest lattice sizes are plotted for all three values of γ. (An individual histogram at $\gamma = 0$ is shown in [3].) Again, there is no indication of a discontinuity signal. Such an observation was made already in the study of the SH lattice (at $\gamma = 0$) in

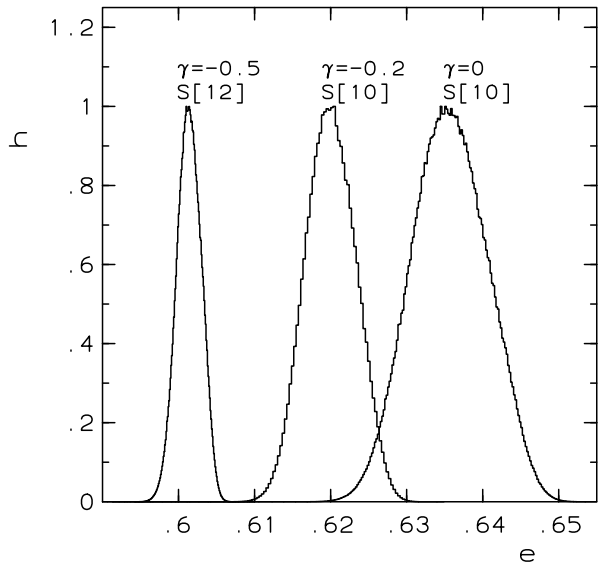

Figure 3: Pseudo-histograms vs e for lattices (from left to right) $S\,[12]$ ($\gamma = -0.5$), $S\,[10]$ ($\gamma = -0.2$) and $S\,[10]$ ($\gamma = 0$) at their respective peak positions of the specific-heat and normalized to unit maximum.

[2].

Also the individual histograms show no two-peak structure. Actually, if the statistics is small, spurious signals may appear, but with increasing statistics they always vanished. (They also were not at consistent positions.) Finally we mention, that there are studies at established but weak first order transitions (the 2D 5-state Potts model) on similar spherelike lattices, where a two-state signal has been observed clearly [46]. Therefore we find no indication, that the particular kind of lattice studied here has a tendency to smear out weak two-state signals.

A two-peak distribution is an indicator of a possible $1^{\rm st}$ order transition. However, in order to establish this order one should also find further signals for coexistence of phases like FSS consistent with $\nu = 1/D = 1/4$, correct scaling of the minimum between the peaks (suppressed due to the 3D interface) in the distribution and tunneling probability $\propto \exp\left(-2\sigma L^3\right)$. Up to now no consistent observations of that kind have been made in the U(1)

theory for the toroidal lattices, where one finds two-state signals.

Within the scope of lattice sizes studied here we are therefore led to assume a 2^{nd} order behavior for $\gamma \leq 0$. The subsequent scaling analysis leads to results fully supporting this assumption.

In Tables 3 and 4 we summarize our results for the extrema values and positions of the cumulants and of the positions of the closest Fisher zeros. The analysis of these data is discussed in the subsequent sections.

Table 3: Extrema positions of the cumulants and the real part of the positions of the closest Fisher zeros.

γ	N	$\beta(c_V)$	$\beta(V_{CLB})$	$\beta(U_4)$	$\mathrm{Re}(z_0)$
0	4	1.0027(3)	0.9990(4)	1.0051(3)	1.0047(4)
	6	1.0151(2)	1.0148(1)	1.0156(2)	1.0156(2)
	8	1.0179(1)	1.0179(1)	1.0182(1)	1.0182(1)
	10	1.0183(1)	1.0183(1)	1.0185(1)	1.0185(1)
-0.2	4	1.1473(6)	1.1422(5)	1.1512(11)	1.1514(12)
	5	1.1588(4)	1.1574(5)	1.1607(5)	1.1608(5)
	6	1.1640(3)	1.1634(3)	1.1652(7)	1.1650(12)
	7	1.1664(4)	1.1662(4)	1.1675(4)	1.1677(2)
	8	1.1681(1)	1.1680(1)	1.1685(3)	1.1684(3)
	9	1.1688(1)	1.1687(1)	1.1690(1)	1.1690(1)
	10	1.1695(1)	1.1695(1)	1.1698(2)	1.1697(2)
-0.5	4	1.4067(7)	1.3987(10)	1.4126(15)	1.4070(42)
	5	1.4202(7)	1.4177(8)	1.4239(13)	1.4246(17)
	6	1.4270(6)	1.4262(6)	1.4291(5)	1.4292(7)
	7	1.4307(4)	1.4304(4)	1.4320(6)	1.4318(5)
	8	1.4325(2)	1.4324(2)	1.4328(3)	1.4328(3)
	9	1.4340(7)	1.4339(8)	1.4354(22)	1.4353(4)
	10	1.4346(2)	1.4345(2)	1.4349(2)	1.4349(2)
	12	1.4359(6)	1.4359(6)	1.4366(1)	1.4365(1)

4.2.2 Fisher zeros

The results for the imaginary part of the position z_0 of the Fisher zero closest to the β axis are given in Table 5. Although we tried fits including further background contributions it turned out that the form (24) is sufficient.

Table 4: Extrema values of the cumulants and the imaginary part of the positions of the closest Fisher zeros.

γ	N	c_V	V_{CLB}	U_4	$\mathrm{Im}(z_0)$
0	4	1.85(1)	-0.142(1)E-02	2.77(1)	0.0300(5)
	6	3.93(5)	-0.362(5)E-03	2.67(2)	0.0066(2)
	8	6.75(14)	-0.157(3)E-03	2.61(3)	0.0024(1)
	10	9.47(23)	-0.792(20)E-04	2.65(2)	0.0013(1)
-0.2	4	1.22(1)	-0.982(6)E-03	2.83(1)	0.0388(10)
	5	1.63(1)	-0.395(3)E-03	2.81(1)	0.0185(4)
	6	2.07(3)	-0.201(3)E-03	2.82(2)	0.0112(14)
	7	2.54(5)	-0.117(2)E-03	2.80(4)	0.0063(3)
	8	3.08(4)	-0.755(9)E-04	2.80(2)	0.0043(2)
	9	3.54(9)	-0.503(12)E-04	2.75(5)	0.0029(2)
	10	4.22(13)	-0.371(11)E-04	2.71(8)	0.0020(2)
-0.5	4	0.76(1)	-0.647(3)E-03	2.89(1)	0.0578(32)
	5	0.95(1)	-0.246(3)E-03	2.88(1)	0.0271(11)
	6	1.16(1)	-0.121(1)E-03	2.85(2)	0.0150(11)
	7	1.36(1)	-0.673(8)E-04	2.83(1)	0.0087(2)
	8	1.62(6)	-0.427(16)E-04	2.72(6)	0.0053(4)
	9	1.69(5)	-0.258(8)E-04	2.87(6)	0.0046(5)
	10	1.98(8)	-0.188(8)E-04	2.78(5)	0.0030(2)
	12	2.26(12)	-0.946(49)E-05	2.78(12)	0.0019(2)

Table 5: Results for ν from individual fits to $\mathrm{Im}\, z_0$ according to (24).

γ	ν	$\chi^2/d.f.$
0	0.345(3)	4.7
-0.2	0.378(7)	0.3
-0.5	0.368(8)	0.8

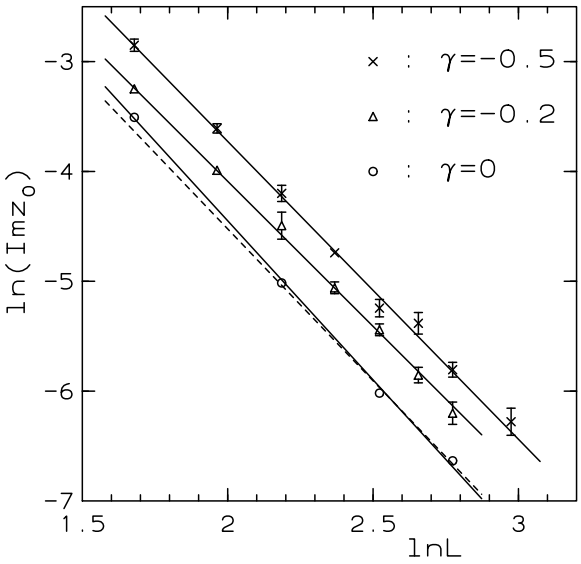

Figure 4: Log-log Plot for $\mathrm{Im}\, z_0$ vs L with individual fits for each γ. At $\gamma = 0$ the full line denotes our fit to all N, the dotted line a fit to data for $N \geq 6$. For $\gamma < 0$ no visible difference would be seen.

In Fig. 4 we show individual fits for each γ. For $\gamma = 0$ we distinguish two lines: the fit to all N and one to data for $N \geq 6$. In particular for $\gamma = 0$ the $N = 4$ data seems to be outside the overall behavior, indicating that at this lattice size the asymptotic behavior is not yet seen. According to our interpretation, we expect the value $\gamma = 0$ to be closest to a tricritical point, which may explain the larger deviations as compared to the other values of γ.

A joint fit to the data for all three γ-values with universal ν but individual proportionality factors gives $\nu = 0.354(3)$ at a $\chi^2/d.f.$ value of 2.7; including only data with $N \geq 5$ we obtain $\nu = 0.368(5)$ ($\chi^2/d.f. = 0.98$). Finally if we restrict the fit to the data with $N \geq 6$ we find $\nu = 0.365(8)$ at a ($\chi^2/d.f$ =1.05). This last fit we consider to be the most reliable determination of ν (a corresponding plot may be found in [3]).

It is interesting to compare the absolute positions of the zeros for different values of γ in Fig. 5. We find that the zeros are generally closer to the real

axis for γ closer to 0. This indicates, that asymptotic scaling sets in somewhat later (at larger lattices) at more negative values of γ. This correlates with the peak values of the specific-heat, as will be discussed below in the discussion of the cumulants.

The results for the real parts of the Fisher zero positions will be discussed together with the pseudocritical values.

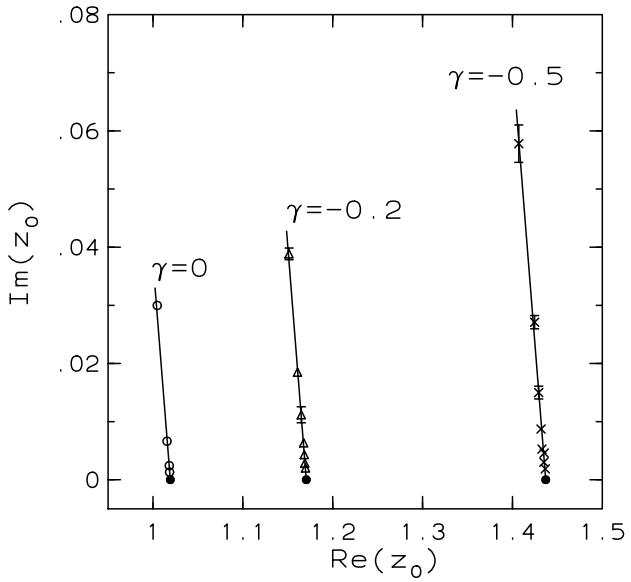

Figure 5: Positions of the closest Fisher zeros for all lattice sizes and all γ.

4.2.3 Cumulant values

Figures 6 and 7 exhibit $\langle e \rangle$ and c_V in the pseudocritical range, and Fig. 8 gives an example for the behavior of V_{CLB}. The inserts in Fig. 7 demonstrate, that the peak values of the specific-heat grow slower than the volume and that c_V/V approaches zero in the thermodynamic limit, indicating a 2^{nd} order PT.

Our ansatz

$$c_{V,max}(L) = a(\gamma) + b(\gamma) L^{2/\nu(\gamma)-4} \tag{31}$$

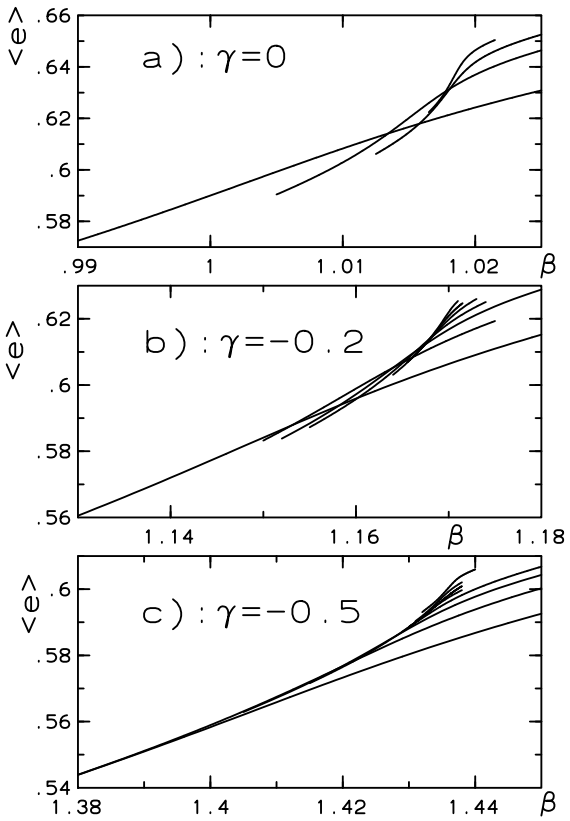

Figure 6: Values of $\langle e \rangle$ vs β around the pseudocritical points for the three values of γ and for all lattice sizes: (a) $\gamma = 0$, $N = 4, 6, 8, 10$; (b) $\gamma = -0.2$, $N = 4, 5, 6, 7, 8, 9, 10$; (c) $\gamma = -0.5$, $N = 4, 5, 6, 7, 8, 9, 10, 12$.

for the scaling behavior (14) (with Josephson's law relating α with ν) allows for a background constant. We performed various fits restricting the coefficients in different ways. It turned out, that one should not omit the background constant $a(\gamma)$. If one does, then the fits become size dependent and have worse χ^2 if all lattice sizes are included and better if one omits the small lattices. We therefore allow for such a background parameter and include all lattices sizes in the fits.

If we leave a, b, and ν $\gamma-$dependent we get consistent results with ν varying between 0.361 and 0.404 (cf. Table 6). If we enforce a γ-independent value of ν we find $\nu = 0.378(4)$ and the reasonable $\chi^2 = 2.2$ but different values for the background parameters.

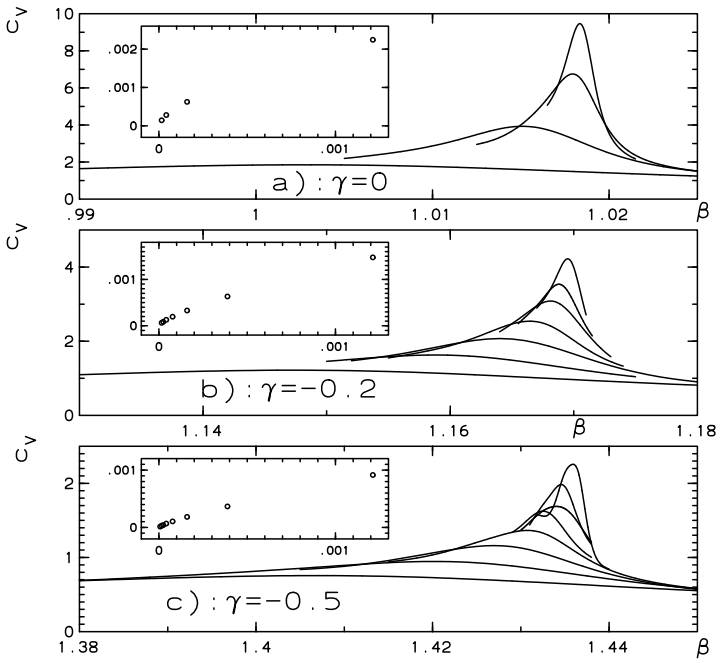

Figure 7: Values of c_V vs β around the pseudocritical points for the considered values of γ and for all lattice sizes: (a) $\gamma = 0$, $N = 4, 6, 8, 10$; (b) $\gamma = -0.2$, $N = 4, 5, 6, 7, 8, 9, 10$; (c) $\gamma = -0.5$, $N = 4, 5, 6, 7, 8, 9, 10, 12$. The inserts exhibit the peak values c_V/V vs $1/V$ demonstrating their approach towards 0 for $V \to \infty$.

Table 6: Results of the fit to c_V according to (31).

γ	ν	$a(\gamma)$	$b(\gamma)$	$\chi^2/d.f.$
0	0.361(6)	0.07(18)	0.136(34)	2.3
-0.2	0.374(6)	0.35(9)	0.090(20)	0.3
-0.5	0.404(9)	0.10(10)	0.132(44)	1.0

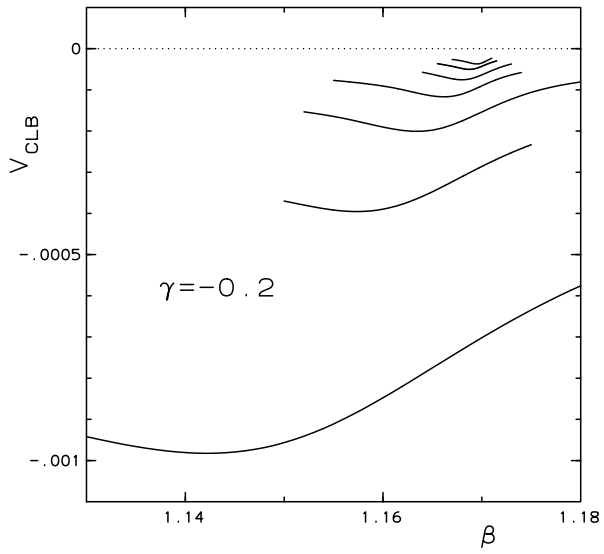

Figure 8: V_{CLB} vs β for all lattices sizes studied at $\gamma = -0.2$. For 1^{st} order PTs the values at the minima should asymptotically approach a nonzero constant.

Fig. 9 is a log-log plot for c_V and the results of the fits (Table 6). The increase of the value for ν with decreasing γ indicates that the behavior of c_V is not yet asymptotic. We observed already in the discussion of the Fisher zero that scaling appears to be retarded towards more negative values of γ. Below (in 4.2.5) we try to correct for this fact by introducing a phenomenological scaling variable. Indeed we find a consistent scaling behavior of the specific-heat maximum corresponding to a value of ν as determined in sect. 4.2.2.

For the CLB-cumulant we found that a fit to the FSS behavior in the form

$$V_{CLB,min}(L) = \left(a(\gamma) + b(\gamma)L^{2/\nu(\gamma)-4}\right) L^{-4} \tag{32}$$

– in the spirit of the correction term in the specific-heat (31) – appears to be suitable. Fig. 10 and Table 7 show our result. The consistency with the results for c_V is remarkable.

The values of V_{CLB} clearly tend to vanish in the thermodynamic limit

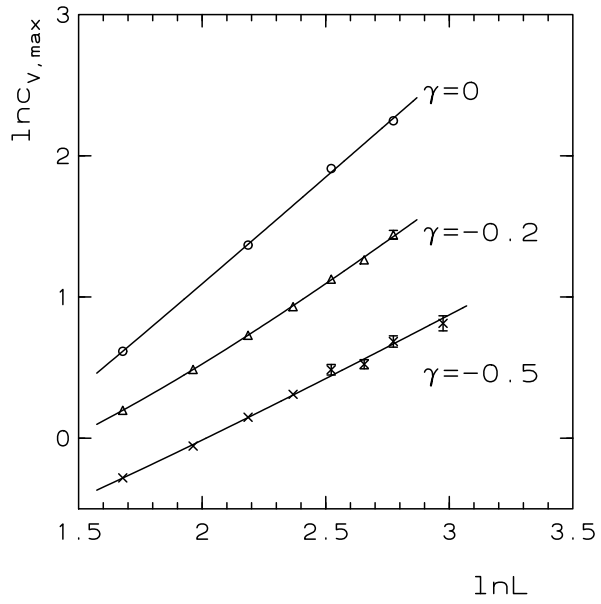

Figure 9: This is a log-log plot of specific-heat c_V vs L together with the fit results to form (31) and parameter values from Table 6.

as expected for 2nd order transitions. It was unexpected, that the scaling analysis led to sensible results in good agreement with the results for the specific-heat. (Note that the CLB-cumulant is a 4th order moment and therefore in principle much more error-prune. For the – in comparison to spin model simulations – low statistics one cannot put too much confidence in this quantity.)

Table 7: Results for the fit of $V_{CLB,min}$ according (32).

γ	ν	$a(\gamma)$	$b(\gamma)$	$\chi^2/d.f.$
0	0.361(6)	-0.23(1)	-0.071(19)	2.3
-0.2	0.365(6)	-0.41(5)	-0.034(9)	0.3
-0.5	0.396(9)	-0.22(5)	-0.054(19)	1.1

If we omit lattice sizes $N < 6$ the χ^2 improves, but the values of ν do not

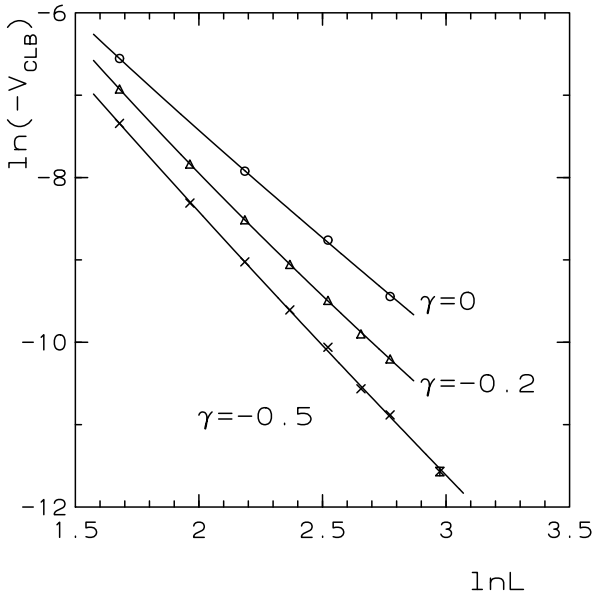

Figure 10: A plot of $\ln(-V_{CLB})$ vs $\ln L$ for all three value of γ, comparing with the fit according to (32).

change much. Like for the specific-heat we notice an increase of ν fit-values with more negative γ which we interpret as due to the retarded FSS.

The data for U_4 show too little size dependence (or have too large errors) to produce a trustworthy fit to the expected leading scaling behavior (16),

$$U_{4,min}(L) = a(\gamma) + b(\gamma)L^{4-2/\nu}. \tag{33}$$

A joint fit to all data ($\chi^2/d.f.$=1.1) gives $\nu = 0.35(3)$ and values of $a = 2.60(3), 2.79(2), 2.81(2)$ which are, however, clearly different from the value 1 expected at a 1^{st} order PT.

4.2.4 Pseudocritical values

Let us denote our four definitions for pseudocritical values by $\beta_c^{(i)}(L)$ (where $i = 1 \ldots 4$ stands for the peak positions of c_V, V_{CLB} and U_4 and $\mathrm{Re}\, z_0$, respectively). In the fits we allow for the form

$$\beta_c^{(i)}(L) = \beta_c + a_i L^{-\lambda}. \tag{34}$$

For each γ we fit simultaneously to all types i for a unique β_c and λ but individual values a_i. We find that allowing for another term $O(L^{-2})$ — as it is motivated from the possible contribution of the curvature or lattice inhomogeneities and as it seemed to be necessary for the analysis of the SH results in [2] — does not improve the χ^2 significantly.

Table 8: Results of the fits to the finite-size dependence of the four definitions of pseudocritical points according to (34).

γ	β_c	$1/\lambda$	$\chi^2/d.f.$
0.	1.0190(1)	0.321(7)	5.8
-0.2	1.1709(2)	0.386(10)	1.6
-0.5	1.4381(1)	0.472(12)	2.5

Table 8 gives the fit values for the pseudocritical points and $1/\lambda$. It is not generally true, that $\lambda = 1/\nu$ (cf. the discussion in [55]) and indeed a recent study indicated a different value for the 2D Ising model on spherelike lattices [44]. Accepting this *caveat* we still find numbers of similar size. If we allow for a correction term $O(L^{-2})$ due to the background curvature of our lattices and fix $\lambda = 1/0.37$ (i.e. at a value $1/\nu$ suggested from the other data) the fit is of comparable quality with compatible values for $\beta_c(\gamma)$ and the fit curves in the plots are indistinguishable by eye.

Altogether the errors on the pseudocritical points are larger but the fits are not very satisfying (cf. Fig. 11 as an example; the data and fits for the other γ-values look similar). The value of λ is not stringently determined by the data (or the theory).

4.2.5 Scaling consistency

At finite lattices there are always corrections to FSS, depending on size, geometry, topology and of course details of the action and the observables. Since $\mathrm{Im}\, z_0$ gives the cleanest FSS signal, we use it as a phenomenological scaling variable

$$x \equiv \mathrm{Im}\, z_0 \tag{35}$$

and study in this section the other observables as functions of x. (Notice that x is defined from the data!) That provides us on one hand with a consistency

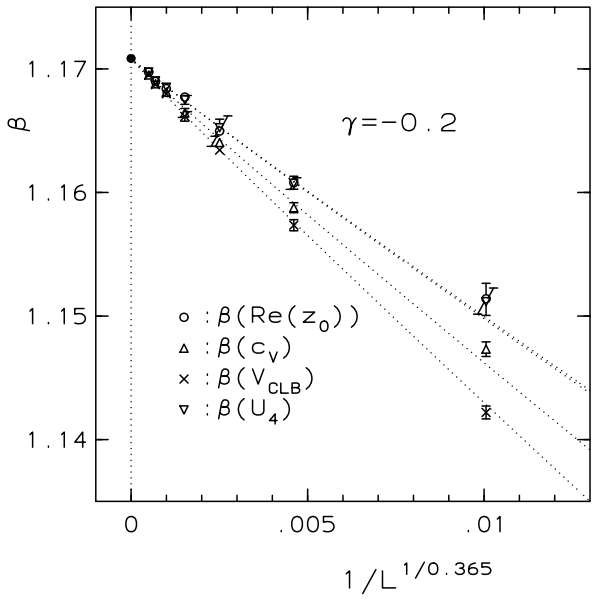

Figure 11: Fits to the data (for $\gamma = -0.2$) for the pseudocritical points (according to the four different definitions described). We use the abscissa variable $L^{-1/\nu}$ (for the preferred value $\nu = 0.365$) in order to emphasize the nontrivial dependence.

check for our results. On the other hand this assumption allows us to bring together and combine results from different values of γ.

Assuming the FSS relation $x \simeq L^{-1/\nu}$ (i.e. for $\mathrm{Im}\, z_0$) we expect e.g. for the specific-heat the behavior (cf. (14))

$$c_{V,max}(L) \simeq a + L^{2/\nu-4} \simeq a + bx^{-2}L^{-4}, \tag{36}$$

where we – as discussed – allow for the additive constant to represent the unknown background. Fig. 12 shows the peak values of the specific-heat for the data vs $x^{-2}L^{-4}$ together with the result of a linear fit to the data for $N \geq 5$. For this fit we had to assume different values of the background constant $a = 0.22, 0.55, 0.40$ for different $\gamma = 0, -0.2, -0.5$. The plot demonstrates the consistency of the FSS of the specific-heat values with that of $\mathrm{Im}\, z_0$. This is not surprising, since these quantities have a close relationship as discussed in sect. 3.2.2.

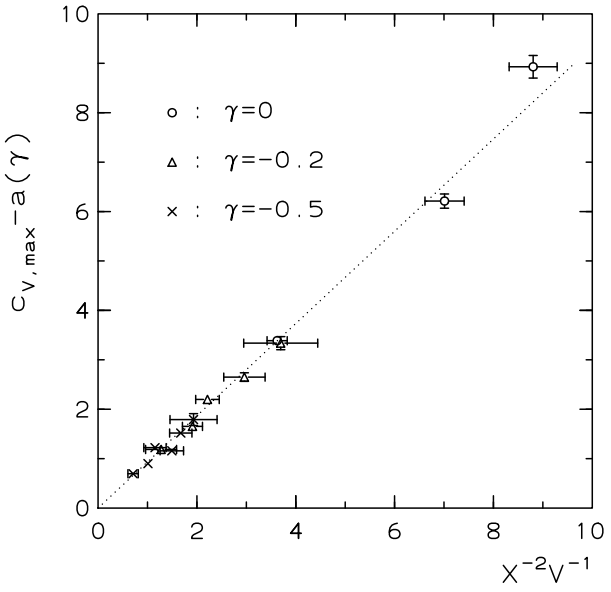

Figure 12: A plot of the peak values of the specific-heat (all γ, all lattices sizes) vs $1/(x^2L^4)$ (x is the phenomenological scaling variable defined in (35); the corresponding error bars are shown as well. The line represents a linear fit.

4.2.6 Summary of the fit results

The cleanest and most consistent results on FSS come from the imaginary part of the closest Fisher zero positions and suggest a value $\nu = 0.365(8)$.

The peak values of the various cumulants are generally consistent with $\nu \simeq 0.35 \ldots 0.40$ although they seem to prefer larger values of ν towards more negative values of γ; this may be explained by later onset of scaling. Allowing for a smooth background (in the neighborhood of the peak) like a constant added to the specific-heat improves the consistency of the scaling.

Even the pseudocritical positions — although with less predictive power due to the uncertainty of the relation of the shift exponent λ to the inverse critical exponent $1/\nu$ — show scaling with values of $1/\lambda$ at least roughly of the same magnitude.

In general we find better scaling behavior than for the more "edgy" lattices types SH studied in [2]. Corrections to FSS due to the curvature (which

may be of $O(L^{-2})$) do not seem to be necessary.

5 Conclusion

After 17 years [1] of development it has now been possible to obtain a consistent picture of the scaling behavior in the pure compact U(1) lattice gauge theory at the confinement-Coulomb phase transition. Using a radically new kind of finite lattices, modern FSS methods and substantial computer power we have found a consistent picture of the scaling behavior of several bulk observables. Within the limits of numerical evidence, our analysis strongly suggests the existence of a non-Gaussian fixed point with ν distinctly different from 1/2 (Gaussian value) or 1/4 ($1^{\rm st}$ order transition). Its universality class extends in the $\beta - \gamma$ plane along the phase transition line at negative γ, but includes also the Wilson action, $\gamma = 0$.

This implies that using RG methods, one can construct a unitary continuum field theory in 4D which is neither asymptotically free nor trivial. As we point out in [3], this holds also for several theories related to the U(1) lattice theory by duality transformations. Thus rather than being an exercise ground for lattice QCD, the pure compact U(1) lattice gauge theory at its phase transition defines a sort of quantum field theory in 4D which is not used either in the Standard Model nor in its presently known extensions.

The natural question is whether these novel features of the U(1) lattice theory might be related to the difficulties encountered in its numerical investigation. The strongly interacting monopole loops are an obvious candidate for concern. The previous studies using the surface of the 5D cubic lattice [2], as well as our present results, suggest that the topology of the finite lattice is crucial. For $\gamma \leq 0$ the two-state signal vanishes on lattices with spherelike topology. However, this fact alone does not yet confirm the speculations that the winding monopole loops are the culprits. A more detailed information about the field configurations, and more experience with various lattices and boundary conditions are required. It could be that the question is indeed more than technical and its pursuit might lead to a deeper understanding of the non-Gaussian fixed point.

Acknowledgments: We wish to thank Ch. Hoelbling and U.-J. Wiese for discussions. The computations have been performed in part on the CRAY-YMP of HLRZ Jülich and the Parallel Compute Server of KFU Graz. The

work has been supported by Deutsches BMBF.

Appendix: Lattice details

The lattice types SH[N] (the surface of an N^5 hypercube) and S[N] have the same link connectivity structure. The lattice is build from plaquettes with 4 links each. Not all sites have 8 links, not all links are bordering 6 plaquettes, and not all plaquettes are faces of exactly four 3D cubes, as it is the case for the hypertorus. All 3D cubes are bordering exactly four 4D cubes.

Let us denote the total number of sites by n_s, and the number of sites with i links by $n_{s,i}$. A corresponding notation holds for the links and plaquettes. We have

sites:	n_s	$= 10(N-1)^4 + 20(N-1)^2 + 2$
	$n_{s,5}$	$= 32$
	$n_{s,6}$	$= 80(N-1) - 80$
	$n_{s,7}$	$= 80(N-1)^2 - 160(N-1) + 80$
	$n_{s,8}$	$= 10(N-1)^4 - 60(N-1)^2$
		$+80(N-1) - 30$
links:	n_l	$= 40(N-1)^4 + 40(N-1)^2$
	$n_{l,4}$	$= 80(N-1)$
	$n_{l,5}$	$= 160(N-1)^2 - 160(N-1)$
	$n_{l,6}$	$= 40(N-1)^4 - 120(N-1)^2$
		$+80(N-1)$
plaquettes:	n_p	$= 60(N-1)^4 + 20(N-1)^2$
	$n_{p,3}$	$= 80(N-1)^2$
	$n_{p,4}$	$= 60(N-1)^4 - 60(N-1)^2$
3D cubes:	n_{3c}	$= 40(N-1)^4$
4D cubes:	n_{4c}	$= 10(N-1)^4$

For example, for $N = 12$ one has $n_s = 148832 \simeq (19.6^4) \simeq V$.

The number of plaquettes with just three 3D cubes (as well as the corresponding numbers for links and sites) is suppressed relative to the leading terms in $O(1/N^2)$. This is typical for contributions due to curvature. We may say that the lattice becomes locally flat with $O(1/N^2)$.

Contrary to the usual hypercubic torus this lattice is not self-dual. Possible monopole loops live on the dual lattice SH', which does have a few ($n_{p,3}$) plaquettes of 3 links in addition to the usual ones.

Euler's relation for spherelike lattices (of the type discussed, i.e. without

further holes) is

$$n_s - n_l + n_p - n_{3c} + n_{4c} = 2 \tag{37}$$

(whereas it is zero for the torus).

The lattice SH — in analogy to the 2D situation — may be imagined as an ensemble of 10 hypercubic lattices, glued together at their boundaries. The lattice S is constructed by a projection of SH from its center onto the unit sphere S^4.

References

[1] M. Creutz, L. Jacobs, and C. Rebbi, Phys. Rev. D **20**, 1915 (1979).

[2] C. B. Lang and T. Neuhaus, Nucl. Phys. B (Proc. Suppl.) **34**, 543 (1994); Nucl. Phys. B **431**, 119 (1994).

[3] J. Jersák, C. B. Lang, and T. Neuhaus, preprint UNIGRAZ-UTP-29-05-96, unpublished.

[4] T. Banks, R. Myerson, and J. Kogut, Nucl. Phys. B **129**, 493 (1977).

[5] M. E. Peskin, Ann. Phys. **113**, 122 (1978).

[6] W. Janke and H. Kleinert, in: *Proc. Conf. and Workshop on Frontiers in Nonperturbative Field Theory, Eger, Hungary, August 18-23, 1988*, edited by Z. Horvath, L. Palla and A. Patkós (World Scientific, Singapore, 1989), p.279.

[7] H. Grosse, in *New Developments in Mathematical Physics, Acta Phys. Austriaca Suppl. XXIII*, edited by E. H. Mitter and L. Pittner (Springer, Wien, 1981), p. 627.

[8] K. Osterwalder and E. Seiler, Ann. Phys. **110**, 440 (1978).

[9] C. B. Lang, Phys. Rev. Lett. **57**, 1828 (1986); in *Lattice Gauge Theory 1986*, edited by H. Satz, I. Harrity, and J. Potvin (Plenum, New York, 1987), p. 195; Nucl. Phys. B **280**, 255 (1987).

[10] K. G. Wilson, Phys. Rev. D **10**, 2445 (1974).

[11] A. H. Guth, Phys. Rev. D **21**, 2291 (1980).

[12] J. Fröhlich and T. Spencer, Commun. Math. Phys. **83**, 411 (1982).

[13] A. M. Polyakov, Phys. Lett. B **59**, 82 (1975).

[14] R. Savit, Phys. Rev. Lett. **39**, 55 (1977).

[15] J. Glimm and A. Jaffe, Commun. Math. Phys. **56**, 195 (1977).

[16] T. A. DeGrand and D. Toussaint, Phys. Rev. D **22**, 2478 (1980).

[17] J. S. Barber, Phys. Lett. B **147**, 330 (1984); J. S. Barber, R. E. Shrock, and R. Schrader, Phys. Lett. B **152**, 221 (1985); J. S. Barber and R. E. Shrock, Nucl. Phys. B **257**, 515 (1985).

[18] B. Lautrup and M. Nauenberg, Phys. Lett. **95B**, 63 (1980).

[19] G. Bhanot, Phys. Rev. D **24**, 461 (1981).

[20] T. A. DeGrand and D. Toussaint, Phys. Rev. D **24**, 466 (1981).

[21] K. J. M. Moriarty, Phys. Rev. D **25**, 2185 (1982).

[22] J. Jersák, T. Neuhaus, and P. M. Zerwas, Phys. Lett. B **133**, 103 (1983).

[23] G. Bhanot, Nucl. Phys. B **205 [FS5]**, 168 (1982).

[24] H. G. Evertz, J. Jersák, T. Neuhaus, and P. M. Zerwas, Nucl. Phys. B **251 [FS13]**, 279 (1985).

[25] D. P. Landau and R. H. Swendsen, Phys. Rev. Lett. **46**, 1437 (1981).

[26] B. Berg and T. Neuhaus, Phys. Lett. B **267**, 249 (1991); Phys. Rev. Lett. **68**, 9 (1992).

[27] A. N. Burkitt, Nucl. Phys. B **270 [FS16]**, 575 (1986).

[28] R. Gupta, M. A. Novotny, and R. Cordery, Phys. Lett. B **172**, 86 (1986).

[29] A. Hasenfratz, Phys. Lett. B **201**, 492 (1988).

[30] H. W. Hamber, Phys. Rev. D **24**, 941 (1981).

[31] A. C. Irving and C. J. Hamer, Nucl. Phys. B **235 [FS11]**, 358 (1984).

[32] K. H. Mütter and K. Schilling, Nucl. Phys. B **200 [FS4]**, 362 (1982).

[33] K. J. M. Moriarty, J. Phys. G **9**, L33 (1983).

[34] D. G. Caldi, Nucl. Phys. B **220 [FS8]**, 48 (1983).

[35] J. Jersák, T. Neuhaus, and P. M. Zerwas, Nucl. Phys. B **251 [FS13]**, 299 (1985).

[36] C. B. Lang and C. Rebbi, Phys. Rev. D **35**, 2510 (1987).

[37] M. Creutz, Phys. Rev. D **23**, 1815 (1981).

[38] V. Grösch *et al.*, Phys. Lett. B **162**, 171 (1985).

[39] V. G. Bornyakov, V. K. Mitrjushkin, and M. Müller-Preussker, Nucl. Phys. B (Proc. Suppl.) **30**, 587 (1993).

[40] W. Kerler, C. Rebbi, and A. Weber, Phys. Rev. D **50**, 6984 (1994).

[41] W. Kerler, C. Rebbi, and A. Weber, Phys. Lett. B **348**, 565 (1995); Nucl. Phys. B **450**, 452 (1995).

[42] A. Bode, T. Lippert, K. Schilling, and P. Ueberholz, in *in Large scale computational physics on massively parallel computers*, edited by H. J. Herrmann and F. Karsch (World Scientific, Singapore, 1993), p. 147, [Int. J. Mod. Phys. C4 (1993) 1205]; A. Bode, T. Lippert, and K. Schilling, Nucl. Phys. B (Proc. Suppl.) **34**, 1205 (1994); T. Lippert, A. Bode, V. Bornyakov, and K. Schilling, Nucl. Phys. B (Proc. Suppl.) **42**, 684 (1995).

[43] N. H. Christ, R. Friedberg, and T. D. Lee, Nucl. Phys. B **210 [FS6]**, 337 (1982).

[44] Ch. Hoelbling and C. B. Lang, UNIGRAZ-UTP-260296, hep-lat/9602025, to appear in Phys. Rev. B.

[45] J. Jersák, C. Lang, and T. Neuhaus, Nucl. Phys. B (Proc. Suppl.) **42**, 672 (1995).

[46] Ch. Hoelbling, A. Jakovac, J. Jersák, C. B. Lang and T. Neuhaus, Nucl. Phys. B (Proc. Suppl.) **47**, 815 (1996).

[47] A. M. Ferrenberg and R. H. Swendsen, Phys. Rev. Lett. **61**, 2635 (1988); **63**, 1658 (1989); **63**, 1195 (1989);

[48] M. S. S. Challa, D. P. Landau, and K. Binder, Phys. Rev. B **34**, 1841 (1986).

[49] K. Binder, in *Computational Methods in Field Theory*, edited by H. Gausterer and C. B. Lang, Lecture Notes in Physics 409 (Springer-Verlag, Berlin, Heidelberg, 1992), p. 59.

[50] A. M. Ferrenberg and D. P. Landau, Phys. Rev. B**44**, 5081 (1991).

[51] M. E. Fisher, in *Critical Phenomena, Proceedings of the 51th Enrico Fermi Summer School, Varena*, edited by M. S. Green (Academic, New York, 1972).

[52] M. E. Fisher and M. N. Barber, Phys. Rev. Lett. **28**, 1516 (1972).

[53] E. Brézin, J. Physique **43**, 15 (1982).

[54] J. L. Cardy, in *Finite-Size Scaling*, edited by J. L. Cardy (North-Holland, Amsterdam, 1988), p. 1.

[55] M. N. Barber, in *Phase Transitions and Critical Phenomena, Vol. 8*, edited by C. Domb and J. Lebowitz (Academic, New York, 1983), Vol. VIII, Chap. 2, p. 104.

[56] C. N. Yang and T. D. Lee, Phys. Rev. **87**, 404 (1952).

[57] M. E. Fisher, in *Lectures in Theoretical Physics*, edited by W. E. Brittin (Gordon and Breach, New York, 1968), Vol. VIIC, p. 1.

[58] M. Falcioni *et al.*, Phys. Lett. B **105**, 51 (1981).

[59] R. Kenna and C. B. Lang, Nucl. Phys. B **393**, 461 (1993); B **411**, 340 (1994); Phys. Rev. E**49**, 5012 (1994).

[60] H. Gausterer and C. B. Lang, Nucl. Phys. B **455**, 785 (1995).

[61] C. Itzykson, R. B. Pearson, and J. B. Zuber, Nucl. Phys. B **220[FS8]**, 415 (1983).

[62] A. Sokal, Nucl. Phys. B (Proc. Suppl.) **20**, 55 (1991).

[63] F. James, Comput. Phys. Commun. **60**, 329 (1990).